ELSEVIER

Intermetallics 8 (2000) 979–985

Intermetallics

www.elsevier.com/locate/intermet

Two-phase materials for high-temperature service

F.R.N. Nabarro [a,b,*]

[a] *Division of Manufacturing and Materials, CSIR, PO Box 395, Pretoria 0001, South Africa*
[b] *Condensed Matter Physics Research Unit, University of the Witwatersrand, Johannesburg, Private Bag 3, WITS 2050, South Africa*

Received 26 October 1999; accepted 15 February 2000

Abstract

The structures and properties of two families of lattice-coherent composites, those based on γ/γ' Ni_3Al and those based on TiAl/Ti_3Al, are shown to have strong similarities. The coherent system of cubic/tetragonal Y_2O_3–stabilized ZrO_2 is then described, and shown to have strong similarities to the system TiAl/Ti_3Al. The phases γ TiAℓ ($L1_o$) and α_2 $Ti_3A\ell$ (DO_{19}) are not cubic, and their anisotropic thermal expansion may lead to ratcheting creep under conditions of thermal cycling. © 2000 Elsevier Science Ltd. All rights reserved.

Keywords: B. Mechanical properties at high temperatures; D. Phase interfaces; E. Mechanical properties, theory; G. Aero-engine components

1. Introduction

An earlier paper [1] considered the structure and properties of two classes of lattice-coherent composite alloys, the γ/γ' superalloys based on Ni_3Al, and the alloys based on TiAl/Ti_3Al. In each class there are close relationships between the crystal structures, and hence the dislocation structures, of the two phases involved. It is shown that these relationships are very similar in the two classes.

We then consider the ceramic system of ZrO_2 partially stabilized by Y_2O_3, in which colonies of a tetragonal phase form in coherence with a cubic matrix [2–4].

The similarities between the three systems considered suggest that new two-phase systems suitable for high-temperature service may need to show similar structural features.

Since the phases γ TiAℓ ($L1_o$) and α_2 Ti_3 Aℓ (DO_{19}) are not cubic, they have anisotropic thermal expansion. Alloys based on them will therefore suffer ratcheting creep under thermal cycling. The mechanism of ratcheting creep is discussed using a simple model, and it seems likely that ratcheting creep may present serious problems in the system TiAℓ/$Ti_3A\ell$.

2. Summary of the plastic properties of the γ/γ' and TiAl/Ti_3Al structures

We summarize here some of the properties described in more detail in Ref. [1].

2.1. Current superalloys viewed on the scale of the precipitate particles

The structure consists of cubes of the γ' phase, an ordered $L1_2$ structure based on Ni_3Al, stacked in a simple cubic array in a matrix of γ, a disordered face-centred cubic lattice, also nickel-based. The γ' phase occupies about 65% of the volume, so the γ channels between them are less than one sixth of the width of the γ' particles. At working temperatures γ' is the strong phase, and the structure is somewhat analogous to that of a "hard metal". Both phases have high melting points, and close-packed structures which probably lead to low diffusion coefficients.

An important observation is that, e.g. at 1000°C, a creep rate of 10^{-7} s^{-1} occurs in the two-phase structure only under a stress more than twice that which gives the same creep rate in the stronger phase. Over a wide range of temperatures, the flow stress of the γ' phase, but not of the γ phase, anomalously increases with increasing temperature. At room temperature, most of an applied load is carried by the γ phase, which is a ductile material; at high temperatures the γ phase is weak, and

* Tel.: +271171-64420; fax: +27-1133-98262.
E-mail address: dobson@physnet.phys.wits.ac.za (F.R.N. Nabarro).

PII: S0966-9795(00)00030-3

the load is carried by the γ' phase. The unconstrained lattice parameters of the γ and γ' structures usually differ by about 0.3%, but the two phases show lattice coherence after standard heat treatments.

2.2. Current superalloys viewed on the atomic scale

The great strength of the two-phase structure is comparison with either of its components is explained as follows. In both phases, glide occurs in $<1\bar{1}0>$ directions on {111} planes. In the disordered γ phase, with lattice parameter a, the repeat distance, which is the Burgers vector of a single dislocation, is $1/2\ a\ <1\bar{1}0>$. In the ordered γ' structure, the repeat distance is $a\ <1\bar{1}0>$. If a single dislocation of the softer γ phase penetrates into the γ' phase, it trails an anti-phase boundary, and it can move only if an external stress provides the energy of the continuously expanding anti-phase boundary.

Under operating stresses, the dislocations in the γ phase cannot penetrate the γ' phase, which acts as a strong reinforcement. Under overload, the γ dislocations penetrate the γ' particles, providing ductility.

The mobile element in the ordered phase is a superdislocation consisting of two $1/2\ a\ <1\bar{1}0>$ dislocations coupled by a narrow strip of anti-phase boundary. This structure of the mobile superdislocation explains the anomalous temperature dependance of the flow stress of the γ' phase. The superdislocation is only mobile if both $1/2\ a\ <1\bar{1}0>$ components lie on the same close-packed {111} plane. However, the energy of the anti-phase boundary is less if the two dislocations lie on a {001} plane, and elastic anisotropy also drives them into this plane. The leading $1/2\ a\ <1\bar{1}0>$ dislocation therefore tends to cross slip into a {001} plane, locking the superdislocation. Since this $1/2\ a\ <1\bar{1}0>$ dislocation is itself weakly dissociated into Shockley partials, and it does not move readily in the {001} plane which is not close packed, the cross slip is thermally activated. The higher the temperature, the more firmly the superdislocation is locked.

2.3. The system TiAl/Ti_3Al

In the complicated phase diagram of Ti–Al, a region likely to have useful mechanical properties is the two-phase domain containing TiAl and Ti_3Al. Both phases are ordered, and both show slight deviations from the close packing of spherical atoms. The TiAl phase, called γ, has the $L1_o$ structure, a face-centred cubic structure with a slight tetragonal distortion ($c/a = 1.02$) produced by the ordering of Ti and Al atoms into alternating 002 layers. As in the face-centred cubic structure, the glide planes are {111} and the glide directions $<1\bar{1}0>$. In any specific family of glide planes, such as (111), the glide direction $[1\bar{1}0]$ is no longer equivalent to the directions $[01\bar{1}]$ and $[10\bar{1}]$. In the first, the displacement $1/2\ [1\bar{1}0]$ replaces a Ti atom by a Ti atom and an Al atom by an Al atom. It would be expected that the dislocation with Burgers vector $1/2\ [1\bar{1}0]$ would therefore glide freely. In fact (e.g. [5]) the critical shear stress for moving these displocations is not low, and shows an anomalous temperature dependence. The displacements $1/2\ [01\bar{1}]$ and $1/2\ [10\bar{1}]$ replace Ti atoms by Al atoms and Al atoms by Ti atoms. The corresponding dislocations therefore trail anti-phase boundaries, and the mobile element is the superdislocation composed of (e.g.) two $1/2\ [01\bar{1}]$ dislocations coupled by a narrow strip of anti-phase boundary. The analogy with Ni_3Al is clear. Again there is a temperature anomaly of the flow stress, and again the anomaly is explained by the thermally-activated cross slip of screw dislocations. The details of the process are different [6–8]. A screw dislocation $1/2\ [01\bar{1}]$ is trapped in a Peierls valley. It can, by thermal activation, throw forward a loop either on (111) or on $(\bar{1}11)$. If an expanding loop on one of these planes meets a loop on the other plane, a pinning point is formed.

The other phase, Ti_3Al, called α_2, has the close-packed hexagonal DO_{19} structure. The glide plane is the base plane (0001). The glide directions are the close-packed directions $<\bar{2}110>$. The close-packed rows of atoms in these directions are composed alternately of atom sequences ...TiAlTiAlTiAl ... and atom sequences ... TiTiTiTiTiTi ... Dislocations in this plane have a Burgers vector of two interatomic spacings, and the flow stress for glide on this plane shows a normal dependence on temperature. In the two-phase structure, there is lattice coherence between these close-packed planes and the close-packed {111} planes of TiAl. Dislocations of type $a\ [01\bar{1}]$and $a\ [10\bar{1}]$ in the TiAl phase can pass freely into the base plane of Ti_3Al. Those of type $1/2\ a\ [1\bar{1}0]$ are partial dislocations of the base plane of Ti_3Al, and can only pass through the Ti_3Al phase by dragging an anti-phase boundary, or in pairs coupled by a strip of anti-phase boundary. The situation is more complicated than that in γ/γ' Ni_3Al, but clearly there are strong analogies.

The major difference between the two systems is that any of the cube planes {100} can form a coherent interface between the γ and γ' phases in a superalloy, and therefore a three-dimensional structure with cubic symmetry can form. A hexagonal crystal of Ti_3Al has only one close-packed basal plane which can interface with a close-packed plane in TiAl. The resulting two-phase structure therefore essentially layered, a polysynthetic twin consisting of alternate slices of TiAl and Ti_3Al.

3. Zirconia ZrO_2 partially stabilized by yttria Y_2O_3

The high-temperature phase of ZrO_2 containing 4.5 mol% per cent Y_2O_3 has the cubic fluorite structure. A

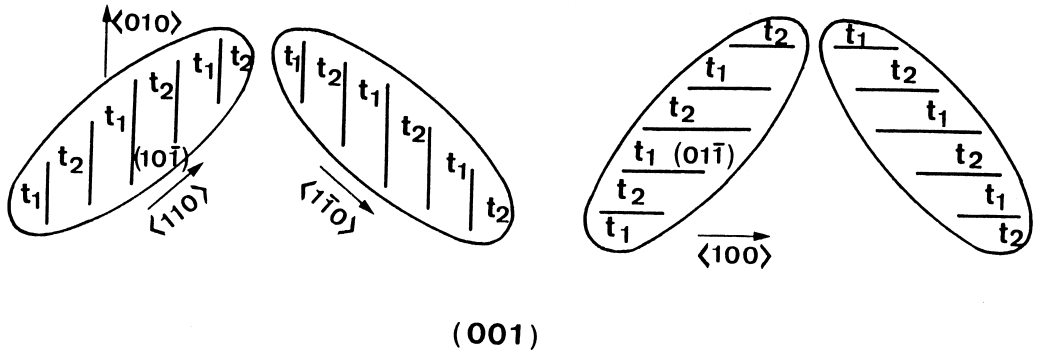

Fig. 1. The four configurations of a coherent tetragonal inclusion of ZrO_2/Y_2O_3 in a cubic matrix which are based on a single pair t_1 and t_2 of the three tetragonal variants t_1, t_2 and t_3 (reproduced by permission from Ref. [2]).

face-centred cube of Zr atoms, with 4 Zr atoms in the unit cell, contains a simple cube of 8 O-atoms. On cooling to about 1600°C, it precipitates a tetragonal phase with $c/a = 1.01$ generated by slight displacements of alternate [001] columns of O-atoms in the ±[001] directions. There are three possible orientations of the c axis of the tetragonal phase giving precipitates labelled t_1, t_2 and t_3 which have their c axes along the a_1, a_2 and a_3 cubic axes, respectively [2] (Fig. 1). To relieve the transformation strain, these variants form in alternating lamellar pairs such as (t_1t_2). The planes of these lamellae contain the a_3 axis. The residual strain energy is further reduced if the boundaries of a (t_1t_2) domain take one of the four forms illustrated in Fig. 1. Since there are three distinct pairs (t_it_j), there are 12 distinct colonies of precipitate, each being a polysynthetic twin reminiscent of the $TiAl/Ti_3Al$ structure. The precipitation hardening is very strong, and is explained by the authors of Ref. [2] by "the fact that matrix dislocations with b = 1/2 [110] are partial dislocations in two of the three t–ZrO_2 precipitate variants that make up the 12 possible colony or fiber variants". While the authors of Ref. [3] describe this system as "ceramic equivalent of γ/γ' Ni-based superalloys", the analogy with the system $TiAl/Ti_3Al$ seems closer, even though both ZrO_2 and γ Ni_3Al have disordered matrices, while in $TiAl/Ti_3Al$ both matrix and inclusion are ordered. However, while cubic symmetry is destroyed in the interaction between a single crystal of the ZrO_2 matrix and each individual colony, it is restored in the collective interaction between the ZrO_2 matrix crystal and its twelve colonies, whereas the Ti_3Al matrix itself has only hexagonal symmetry.

As a result of this, structures based on $TiAl/Ti_3Al$, unlike the other two systems described, are liable to show ratcheting creep in thermal cycling.

4. Creep under thermal cycling

Sections 4.1 and 4.2 give simplified physical discussions of the processes involved in creep under thermal cycling, which may be useful introductions to the formal mathematical treatments which have been published. In Section 4.3 it appears that the data required to estimate the magnitude of the effects in the system $TiA\ell/Ti_3A\ell$ are not all available, but that the effects may well be severe.

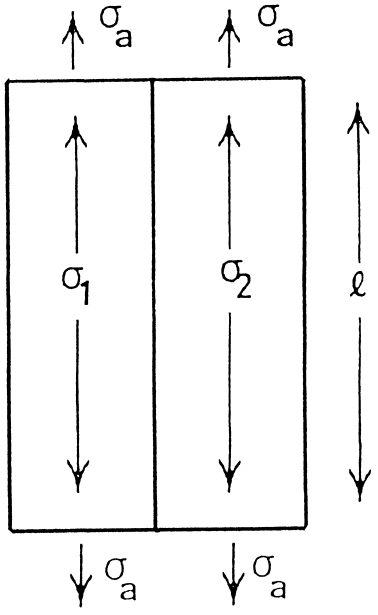

Fig. 2. A bicrystal of an anisotropic material of length ℓ. When the applied stress is σ_a, the stresses in the two components are σ_1 and σ_2.

4.1. Thermal ratcheting creep in an elastic/perfectly plastic bicrystal

As a heuristic model, we take a two-dimensional bicrystal subjected to a small stress σ_a parallel to the join of the two crystals (Fig. 2). At any stage, the stresses in the components are σ_1 and σ_2. The "principle" of de St. Venant requires that

$$\sigma_1 + \sigma_2 = 2\sigma_a. \tag{1}$$

The coefficients of thermal expansion of the two crystals parallel to the axis of stress are α_1 and α_2. We write

$$A = \alpha_1 - \alpha_2. \tag{2}$$

In this heuristic model, we assume that the two crystals have the same Young's modulus E parallel to the stress axis, and the same plastic flow stress σ_f (T), which decreases linearly with temperature from its value σ_R at room temperature T_R to zero at a temperature T_o (which will generally lie above the melting temperature). Thus,

$$\sigma_f(T) = \frac{T_o - T}{T_o - T_R}\sigma_R. \tag{3}$$

We assume (Fig. 3) that the crystals are formed under zero stress at the melting temperature T_M. Initially, differential thermal expansion will produce thermoelastic stresses at a temperature T below T_M given by

$$\sigma_1 = \tfrac{1}{2}EA(T_M - T) \tag{4}$$

and

$$\sigma_2 = -\tfrac{1}{2}EA(T_M - T), \tag{5}$$

as shown by the lines AL and AB in Fig. 3.

These stresses will reach the flow stress at a temperature T_1, given by

$$\tfrac{1}{2}EA(T_M - T_1) = \frac{T_o - T_1}{T_o - T_R}\sigma_R.$$

If we write

$$K = \frac{2\sigma_R}{EA(T_o - T_R)} \tag{6}$$

this gives

$$T_1 = \frac{T_M - KT_o}{1 - K}. \tag{7}$$

Clearly $K > 0$, and it follows from (7) that plasticity will occur above room temperature only if

$$K < \frac{T_M - T_R}{T_o - T_R} < 1. \tag{8}$$

We shall assume this to be the case.

On further cooling from T_1 to room temperature T_R, the stresses follow the plastic lines LM, BC.

The small external stress σ_a is then applied. Crystal 1 remains plastic under stress σ_R, while according to (1) the stress in crystal 2 moves from C to D, with the value

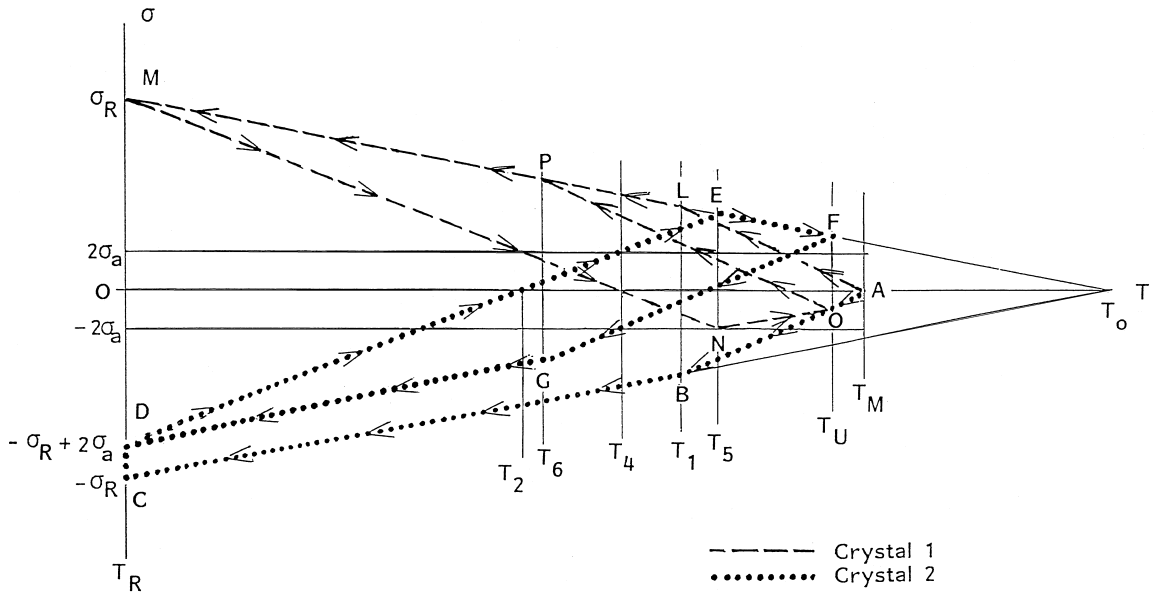

Fig. 3. Stresses during the thermal cycling of a bicrystal. The flow stress at room temperature is σ_R, and decreases linearly with temperature to vanish at a hypothetical temperature T_o. The bicrystal is formed stress-free at the melting temperature T_M. As it cools in the absence of external stress, thermoelastic stresses follow the elastic lines AB, AL, followed by the plastic lines BC, LM. An external stress σ_a is applied at room temperature, and crystal 2 moves to point D. On heating, the crystals follow the elastic lines DE, MN, until crystal 2 becomes plastic along the line EF, terminating at the upper operating temperature T_U. Meanwhile, crystal 1 moves elastically along NO. On cooling, the crystals move elastically along OP and FG, until crystal 1 becomes plastic at P. The crystals then move along PM and GD. Later thermal cycles repeat the stress cycles DEFGD and MNOPM, in which the links EF and PM involve plastic deformation.

$$\sigma_2 = -\sigma_R + 2\sigma_a. \tag{9}$$

The first half-cycle of heating from T_R to an upper working temperature T_U begins with both crystals expanding elastically along the lines DE and MN.

The stress in crystal 2 vanishes at T_2, where that in crystal 1 is $2\sigma_a$, while at T_4 the stress in crystal 1 vanishes and that in crystal 2 is $2\sigma_a$.

Crystal 2 becomes plastic at E, at a temperature T_5 given by

$$-\sigma_R + 2\sigma_a + \tfrac{1}{2}EA(T_5 - T_R) = \frac{T_o - T_5}{T_o - T_R}\sigma_R, \tag{10}$$

which gives

$$T_5 = \frac{2KT_o}{1+K} + \frac{1-K}{1+K}T_R - \frac{4}{1+K}\frac{\sigma_a}{EA}. \tag{11}$$

If the upper operating temperature T_U is below T_5, temperature cycling between T_U and T_R is completely elastic. We now consider the behaviour when T_U is greater than T_5.

Crystal 2, which shed $2\sigma_a$ of its compressive stress on loading at T_R as a result of the plastic yielding of crystal 1, comes to its tensile plastic limit at T_5, and as the temperature increases from T_5 to the upper operating temperature T_U its stress follows the plastic line EF, while, in accordance with (1), the stress in crystal 1 follows the line of opposite slope NO.

At T_U we have

$$\sigma_2 = \sigma_F(T_U) = \frac{T_o - T_U}{T_o - T_R}\sigma_R, \tag{12}$$

while at O, from (1),

$$\sigma_1 = 2\sigma_a - \frac{T_o - T_U}{T_o - T_R}\sigma_R. \tag{13}$$

On cooling from T_U, crystal 1 contracts elastically along OP, until the temperature T_6 is reached at which crystal 1 becomes plastic . Here

$$2\sigma_a - \frac{T_o - T_U}{T_o - T_R}\sigma_R + \tfrac{1}{2}EA(T_U - T_6) = \frac{T_o - T_6}{T_o - T_R}\sigma_R. \tag{14}$$

This gives

$$T_6 = -\frac{2K}{1-K}T_o + \frac{1+K}{1-K}T_U + \frac{4}{1-K}\frac{\sigma_a}{EA}, \tag{15}$$

$$\sigma_1 = \frac{T_o - T_6}{T_o - T_R}\sigma_R$$

$$= \frac{EAK}{2(1-K)}[(1+K)(T_o - T_U) - 4\sigma_a/EA] \tag{16}$$

and

$$\sigma_2 = -\frac{EAK}{2(1-K)}[(1+K)(T_o - T_U) - 4\sigma_a/EAK]. \tag{17}$$

On further cooling to T_R, crystal 1 moves along the plastic line PM, while crystal 2 moves elastically along GD in accordance with (1). Subsequent cycles follow the paths $DEFGD$ and $MNOPM$.

In each cycle, there are two plastic regions. In one region, crystal 1 deforms from P to M, and in the other, crystal 2 deforms from E to F.

While crystal 1 deforms from P to M and crystal 2 from G to D, the two crystals remain of equal length, and the elastic strain remains constant at σ_a/E. The difference in thermal strains $A(T_6 - T_R)$ is accommodated by a plastic extensional strain $A(T_6 - T_R)$ in crystal 1, representing a plastic strain of the length as a whole of $\frac{1}{2}A(T_6 - T_R)$.

Similarly, when crystal 2 deforms from E to F and crystal 1 from N to O, the smaller thermal expansion of crystal 2 is compensated by its plastic extensional strain of $A(T_U - T_5)$, representing a plastic strain of the bicrystal as a whole of $\frac{1}{2}A(T_U - T_5)$.

Thus the total plastic strain of the bicrystal in each thermal cycle is

$$\frac{1}{2}A(T_6 - T_R + T_U - T_5) = A\left[-\frac{2KT_o}{1-K^2} - \frac{T_R}{1+K} + \frac{T_U}{1-K}\right] + \frac{4\sigma_a}{E(1-K^2)}. \tag{18}$$

Again, since $T_U > T_5$, it follows from (11) that the term involving square brackets in (18) is greater than

$$-\frac{4\sigma_a}{E(1-K^2)},$$

so that (18) is always positive.

However, if T_U is finitely greater than T_5, (18) gives a finite strain per cycle even if σ_a is vanishingly small. This unphysical result follows from the assumption that the material is elastic/perfectly plastic. As a result, crystal 1 remains elastic while crystal 2 is plastic during heating from T_5 to T_U, while crystal 1 is plastic and crystal 2 elastic during cooling from T_6 to T_R, however small the positive value of σ_a. If σ_a is given a small negative

value, the shapes of the stress-temperature cycles change discontinuously. To obtain a realistic estimate of the plastic strain per cycle, it is necessary to smooth this abrupt change.

4.2. Relaxation of the elastic/perfectly plastic condition

The result of the previous calculation is determined by situations in which the stress in one crystal is the flow stress $\pm\sigma_f(T)$. Then, if σ_a is very small, it follows from (1) that the stress in the other crystal is very close to $\pm\sigma_f(T)$. It is not realistic to assume that one crystal will be perfectly plastic and the other perfectly elastic. It is more realistic to assume that the two crystals will both deform plastically, the plastic strains in the two being proportional to $(\sigma_a+\sigma_f):(\sigma_a-\sigma_f)$.

Consider the segment EF in Fig. 2. For an increase in temperature δT, crystal 1 would increase in length by $A\ell\delta T$ more than crystal 2 if the two were not connected. This difference is accommodated by a plastic compression of crystal 1 and a plastic extension of crystal 2, the sum of these being $A\ell\delta T$. Thus the plastic compression of crystal 1 is

$$\frac{\sigma_a-\sigma_f}{2\sigma_f}A\ell\delta T, \tag{19}$$

while the plastic extension of crystal 2 is

$$\frac{\sigma_a+\sigma_f}{2\sigma_f}A\ell\delta T. \tag{20}$$

These plastic deformations accommodate the difference of thermal expansions, while there is an overall plastic extension of

$$\frac{\sigma_a}{2\sigma_f}A\ell\delta T. \tag{21}$$

The total plastic strain along EF is then

$$\frac{A\sigma_a}{2}\int_{T_5}^{T_U}\frac{dT}{\sigma_f(T)}=\frac{\sigma_a}{EK}\ell n\frac{T_o-T_5}{T_o-T_U}. \tag{22}$$

Similarly, the total plastic strain along PM is

$$\frac{\sigma_a}{EK}\ell n\frac{T_o-T_R}{T_o-T_6}, \tag{23}$$

and the total plastic strain in a cycle is

$$\frac{\sigma_a}{EK}\ell n\frac{(T_o-T_5)(T_o-T_R)}{(T_o-T_U)(T_o-T_6)}. \tag{24}$$

Now $T_o>T_5$ and $T_6>T_R$, so (29) is always positive. Since σ_a has been assumed small, the terms in σ_a in (11) and (15) may be neglected, and (24) may be written

$$\frac{2\sigma_a}{EK}\ell n\left(\frac{1-K}{1+K}\frac{T_o-T_R}{T_o-T_U}\right). \tag{25}$$

The analysis so far has considered the thermal stresses arising between the crystals with their axes of greatest thermal expansion orthogonal. If the angle between these axes is θ the thermal stresses will be reduced by a factor $\sin^2\theta$. Thus the value of A in (6) should be reduced by a factor $<\sin^2\theta>=\frac{2}{3}$, leading to an effective value of K given by

$$K_{eff}=\frac{3\sigma_R}{EA(T_o-T_R)}. \tag{26}$$

The theory of thermal ratcheting creep in a polycrystal was developed by Anderson and Bishop [9], Greenwood and Johnson [10] and Pickard and Derby [11]. Experimentally, the evidence is limited, but observations on zinc [12] show that the creep rate during thermal cycling may greatly exceed that which occurs under the same load at a steady high temperature.

4.3. Acceleration of creep when thermal stresses do not induce plasticity

The discussion so far has assumed that thermal stresses become so large that the materials becomes fully plastic, and the stressed sample undergoes a finite deformation in each thermal cycle. Anderson and Bishop treated also the case in which the thermal stresses exceed the applied stress but fall below the yield stress.

Then if we assume power-law creep with

$$\dot\varepsilon=R\sigma^n,\ n\approx 4.5, \tag{27}$$

the creep rate in the absence of internal stresses is

$$\dot\varepsilon=R\sigma_a^n. \tag{28}$$

If there are random internal stresses $\pm\sigma_i$ the creep rate is of order

$$\dot\varepsilon=\tfrac{1}{2}R[(\sigma_i+\sigma_a)^n-(\sigma_i-\sigma_a)^n]$$

and, if $|\sigma_i|>>\sigma_a$, this is approximately

$$\dot\varepsilon=nR\sigma_i^{n-1}\sigma_a, \tag{29}$$

a steady creep rate greater than that (28) which would occur in the absence of thermal stresses.

4.4. Thermal cycling in TiAl/Ti_3Al

The physical properties of TiAl have been reviewed by Yoo and Fu [13]. Consider polycrystalline TiAl cycled between 300 and 1200 K. The mean thermal expansion coefficients in this range are about 13.1×10^{-6} K^{-1} along [100] and 11.8×10^{-6} K^{-1} along [001]. A temperature change of 900 K results in a differential thermal expansion strain of about 1.2×10^{-3}. With Young's modulus about 170 GPa, this represents internal stresses of order 200 MPa, leading to resolved shear stresses of order 100 MPa. The critical resolved shear stresses are of order 100–150 MPa. It seems that polycrystalline TiAl cycled between 300 and 1200 K will lie on the borderline between creep accelerated by thermal cycling and thermal ratcheting creep.

Similar data do not seem to be available for Ti_3Al. Since TiAl is very nearly cubic at all temperatures, it seems likely that Ti_3Al polycrystals or TiAl/Ti_3Al two-phase materials thermally cycled in this range will show full thermal ratcheting creep.

5. Summary

Two suggestions are made concerning the likely development of two-phase materials for high-temperature service. Firstly, three systems of current interest have structural features in common, and so it is likely that any successful new system will show similar structural features. Secondly, non-cubic structures, including TiAℓ/$Ti_3A\ell$, will show accelerated creep, probably of important magnitude, when thermally cycled under load.

References

[1] Nabarro FRN. Mater Sci Engng 1994;A184:167.
[2] Heuer AH, Lanteri V, Dominguez-Rodriguez A. Acta Metall 1989;37:559.
[3] Martinez-Fernandez J, Jimenez-Melendo M, Dominguez-Rodriguez A. Acta Metall Mater 1993;41:3171.
[4] Martinez-Fernandez J, Jiminez-Melendo M, Dominguez-Rodriguez A, Cordier P, Lagerlöf KPD, Heuer AH. Acta Metall Mater 1995;43:2469.
[5] Jiao S, Bird N, Hirsch PB, Taylor G. Mat Res Soc Symp Proc 1999;552:KKB.11.1.
[6] Viguier B, Hemker KJ, Bonneville J, Louchet F, Martin J-L. Phil Mag 1995;A71:1295.
[7] Louchet F, Viguier B. Phil Mag 1995;A71:1313.
[8] Jiao S, Bird N, Hirsch PB, Taylor G. Phil Mag 1998;A78:777.
[9] Anderson RG, Bishop JFW. In Inst. of Metals Symp. on Uranium and Graphite, Inst of Metals London, 1962. p. 17.
[10] Greenwood GW, Johnson RH. Proc Roy Soc: London 1965; A283:403.
[11] Pickard SM, Derby B. Acta Metall Mater 1996;38:2537.
[12] Wu MY, Wadsworth J, Sherby OD. Metall Trans 1987;18A:451.
[13] Yoo MH, Fu CL. Metall Mater Trans 1998;29A:49.